RSC Advances

ROYAL SOCIETY OF CHEMISTRY

www.rsc.org/advances

Cite this: DOI: 10.1039/c0xx00000x

www.rsc.org/ RSC Advances

Full Paper

Highly Dispersible Ternary Composites with High Transparency and Ultra Low Dielectric Constants Based on Hyperbranched Polyimide with Organosilane Termini and Cross-linked Polyimide with Silica

Seongku Kim[1], Shinji Ando[2*], and Xiaogong Wang[1*]

Received (in XXX, XXX) Xth XXXXXXXXX 20XX, Accepted Xth XXXXXXXXX 20XX
DOI: 10.1039/b000000x

Flexible insulating materials that are both thermally and mechanically stable, highly transparent, and have low dielectric constants are highly desirable for electronic applications. With these technical needs, a highly disperse inorganic matrix is the most important factor in polyimide-inorganic composites. We report an optimised method for the preparation of a hyperbranched polyimide using $HBPI_{BPADA\text{-}TAP(Si)}$. This method involves modifying the polymer termini by coupling (3-isocyanatopropyl) triethoxysilane to $HBPI_{BPADA\text{-}TAP(OH)}$ via the hydroxyl (–OH) groups at peripheral positions of the polymer chain. Then, based on the $HBPI_{BPADA\text{-}TAP(Si)}$ with silane-modified termini, linear $PI_{6FDA\text{-}APB(Si)}$ and tetraethoxysilane cross-linking agent were used to prepare ternary composites, $PI_{6FDA\text{-}APB(Si)}$_$HBPI_{BPADA\text{-}TAP(Si)}$_$SiO_2$, by sol-gel cross-linking reaction. The dielectric constant (D_k) of $PI_{6FDA\text{-}APB(Si)}$_$HBPI_{BPADA\text{-}TAP(Si)}$-30%_$SiO_2$-20% was very low, 2.04, and the optical transparencies of the ternary hybrid composite films also improved over those of similar composites due to the synergistic interactions between $HBPI_{BPADA\text{-}TAP(Si)}$ and $PI_{6FDA\text{-}APB(Si)}$ that improves phase dispersion. The highest transparency, 95% at 450 nm, was obtained for $PI_{6FDA\text{-}APB(Si)}$_$HBPI_{BPADA\text{-}TAP(Si)}$-30%_$SiO_2$-20%, a significant improvement from that (87%) of the binary composite of $PI_{6FDA\text{-}APB(Si)}$_SiO_2-20%. The glass transition temperature (T_g) of $PI_{6FDA\text{-}APB(Si)}$_$HBPI_{BPADA\text{-}TAP(Si)}$-30%_$SiO_2$-20% is 212.6 °C, which is the highest in the ternary composite series. $PI_{6FDA\text{-}APB(Si)}$_$HBPI_{BPADA\text{-}TAP(Si)}$-40%_$SiO_2$-20% has the largest storage modulus, 2952.0 MPa at 180 °C. The tan δ values of the composite films decreased from 0.96 to 0.73 with increasing $HBPI_{BPADA\text{-}TAP(Si)}$ content. The ternary hybrid composites with densely cross-linked SiO_2 covalent networks developed in this study have improved dielectric, optical, thermal, and mechanical properties. Our fabrication method paves the way to the facile production of high-performance flexible and transparent electronic circuits that could be used in a broad range of applications in future electronics.

*1. *Department of Chemical Engineering, Laboratory of Advanced Materials (MOE), Tsinghua University, Beijing, 100084, P. R. China*
Corresponding author: email wxg-dce@mail.tsinghua.edu.cn
*2. *Department of Chemistry & Materials Science, Tokyo Institute of Technology, Ookayama 2-12-1-E4-5, Meguro-ku, Tokyo, 152-8552, Japan*
Corresponding author: email sando@polymer.titech.ac.jp

Cite this: DOI: 10.1039/c0xx00000x

www.rsc.org/ RSC Advances

Full Paper

Introduction

The rapid development of flexible transparent electronic devices has increased the demand for new materials.[1–9] Colourless and transparent polyimides (PIs) with inorganic component are desirable candidates for use in high-technology devices because they are excellent insulators interlayer dielectrics and because of their optimised properties, such as good flexibility, low dielectric constants, and high thermal, chemical, and mechanical stability.[10–17]

Generally, ideal insulating materials should not only have low dielectric properties, but also be highly transparent, have good mechanical durability and high thermal stability. Therefore, many researchers have designed and demonstrated PIs with these features.[13,18–25] However, there remain several fundamental drawbacks. For example, the opaqueness that originates from organic–inorganic micro phase separation, low inorganic dispersibility, and low toughness and mechanical stability. In addition, composite systems have the drawbacks of the original backbone material that can adversely affect their properties.[19,26–29] We have recently fabricated a novel ternary hybrid system: a hydroxyl terminated hyperbranched polyimide with linear PI/SiO_2[30–32] that has excellent properties, for example, a very low dielectric constant, reduced organic particle size[30–33] and good thermal stability. Additionally, we have reported that by using a flexible organosilane agent nano-sized domains of SiO_2 are formed and that this produces a highly dispersed material.[32,33]

In this study, we report our design of a novel ternary composite system to overcome the drawbacks of existing materials and to improve material performance, for example, improving the organic–inorganic phase dispersion and reducing the interfacial polarisation via strong covalent bonds using a silane-coupling terminus in the ternary system. (3-Aminopropyl) triethoxysilane (APTEOS) was used to modify the termini of the linear PI, and (3-isocyanatopropyl) triethoxysilane (ICTEOS) was used to modify the termini of the hyperbranched PI, $HBPI_{BPADA\text{-}TAP(OH)}$. Modifying the end-groups of the hyperbranched polyimides is an effective way to improve their phase dispersion composition because by adding flexible organosilane terminal groups the polymers become highly soluble and reactive.

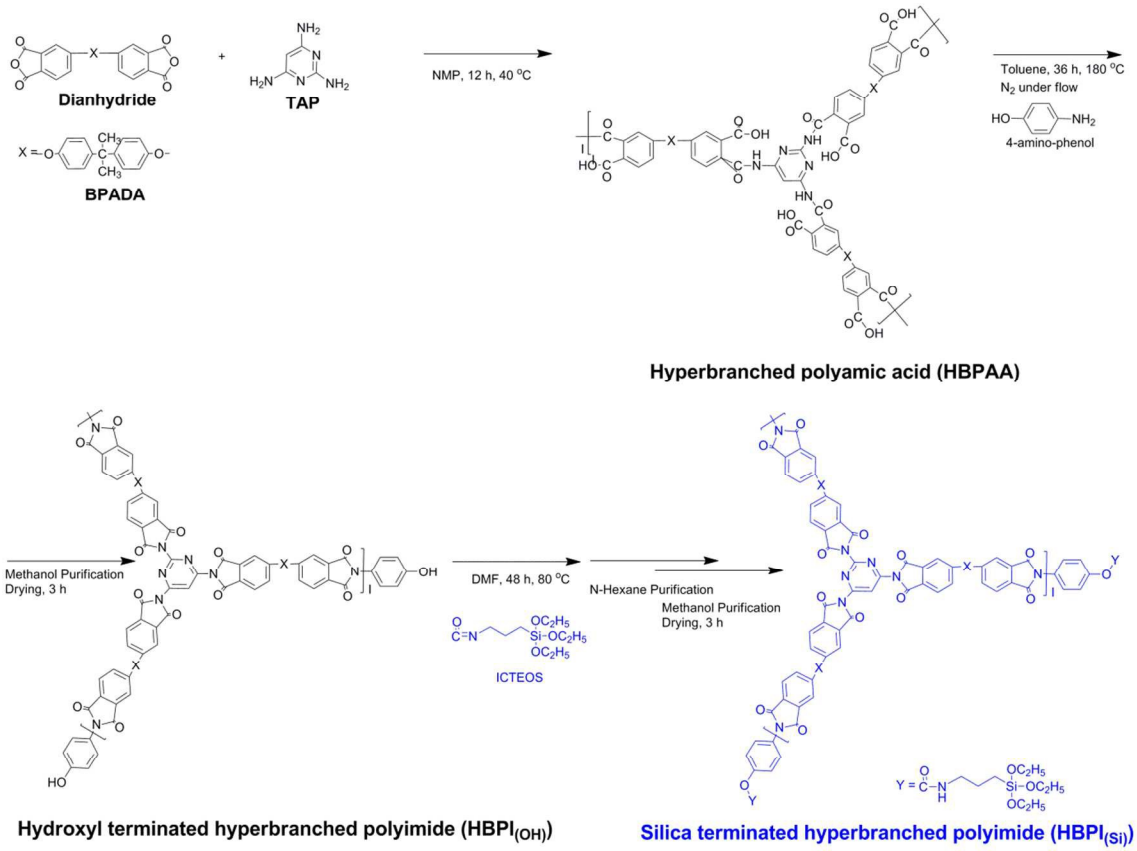

Scheme 1 Synthetic route for the $PI_{6FDA\text{-}APB(Si)}\_HBPI_{BPADA\text{-}TAP(Si)}\_SiO_2$ hybrid ternary composite film

$PI_{6FDA\text{-}APB(Si)}\_HBPI_{BPADA\text{-}TAP(Si)}\_SiO_2$ hybrid ternary composite films with cross-linked structures were prepared by sol-gel cross-

linking reactions. A densely cross-linked structure is beneficial not only to improve the physical properties, in particular the dielectric constants, but also to enhance the phase dispersion by their particular termini linkage. Our fabrication method paves the way for a new and facile production method for high-performance, flexible, and transparent circuits that could have a broad range of applications in flexible electronics. The structures and properties of the composites have been carefully characterised and are reported in the following sections in detail.

Experimental Section

Materials

4,4'-(Hexafloroisopropylidene) diphthalic anhydride (6FDA, 95%), 2,4,6-triaminopyrimidine (TAP, 98%), 1,3-bis(3-aminophenoxy)benzene (APB, 98%), (3-isocyanatopropyl) triethoxysilane (ICTEOS, 98%) and (3-aminopropyl) triethoxysilane (APTEOS, 98%) were purchased from Adamas-Reagent Co. Ltd. 4,4'-Bis(4,4'-isopropylidene diphenoxy) bis-(phthalic anhydride) (BPADA 97%) was purchased from the Sigma-Aldrich Corporation. 4-Amino-phenol was purchased from Tianjin Chem. Eng. Lab. *N, N*-Dimethylacetamide (DMAc, 98%), *N*, *N*-dimethylmethanamide (DMF, 98%), tetrahydrofuran (THF, 98%), n-hexane, methanol and toluene, used as the reaction media, were purchased from Beijing Chemical Works and Alfa Aesar. The solvent *N*-methyl-2-pyrrolidone (NMP, 97%) was purchased from Beijing Modern Eastern Fine Chemical. Hydrochloric acid (HCl) and tetraethoxysilane (TEOS, 98%) were purchased from Alfa Aesar and used without further purification. If not mentioned specifically, the reactants and solvents were used as received without further purification.

Synthesis

The synthetic routes to the materials are shown in **Schemes 1** and **2**, which include the preparation of the silane terminated hyperbranched $HBPI_{BPADA\text{-}TAP(Si)}$ (**Scheme 1**) and the hybrid, ternary composite $PI_{6FDA\text{-}APB(Si)}\_HBPI_{BPADA\text{-}TAP(Si)}\_SiO_2$, film (**Scheme 2**). The preparation details are described as follows. The synthetic methods for both silane terminated linear PAA and binary composite ($PI_{6FDA\text{-}APB(Si)}\_SiO_2$-20%, SD-1) have been described in our previous report.[32]

Silane termini modified hyperbranched polyimide ($HBPI_{BPADA\text{-}TAP(Si)}$). The silane groups at the peripheral positions were then introduced by modification of the hydroxyl (–OH) termini by using (3-isocyanatopropyl) triethoxysilane (ICTEOS), converting $HBPI_{BPADA\text{-}TAP(OH)}$ to $HBPI_{BPADA\text{-}TAP(Si)}$ (**Scheme 1**). Synthesis of the –OH termini hyperbranched polyimides has been described in our previous work.[30] To obtain silane terminated polyimide, in a thoroughly dried 100-ml tri-neck flask, an excess of (3-isocyanatopropyl) triethoxysilane (ICTEOS, 0.29 g, 0.35mmol) was added to a DMF (11.61 g) solution of $HBPI_{BPADA\text{-}TAP(OH)}$ (1.00 g) powder, leading to a solution with 10wt% solid content. The mixture was magnetically stirred at 80 °C for 48 h under nitrogen gas.

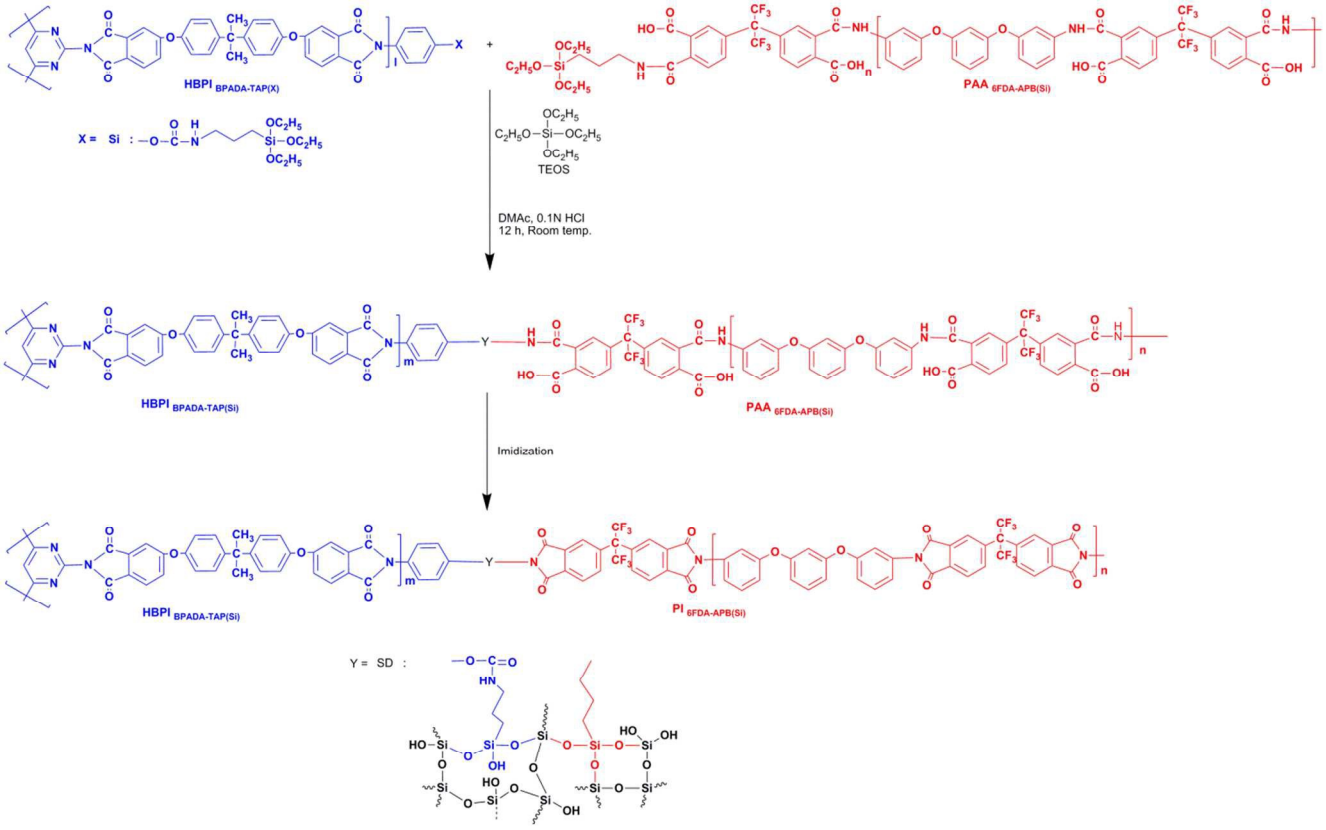

Scheme 2 Synthetic route for the $PI_{6FDA\text{-}APB(Si)}\_HBPI_{BPADA\text{-}TAP(Si)}\_SiO_2$ hybrid ternary composites

The mixed solution of $HBPI_{BPADA\text{-}TAP(Si)}$ was obtained. Firstly, the mixture was poured into n-hexane. Then, it was poured into methanol and the product, a yellow precipitate, formed. This powder was collected by filtration and dried under vacuum at 80 °C for 3 h. Yield = 82%, M_w = 7900, M_n = 2500, PDI (M_w/M_n) = 3.1, ^{1}H NMR (600 MHz, deuterated dimethylsulfoxide), δ (*ppm*): 7.89 (CH, $2H_f$), 7.44–7.21 (CH, $4H_b$, $2H_e$), 7.29 (CH, $2H_d$), 7.11 (CH, $2H_g$), 7.02 (CH, $4H_c$), 6.82 (CH, $2H_h$), 4.97 (NH, $1H_j$), 4.12 (CH_2, $6H_n$), 3.75 (CH, $1H_i$), 3.47 (CH_2, $2H_k$), 1.67–1.60 (CH_3, $6H_a$, CH_2, $2H_l$), 1.15 (CH_3, $9H_o$), 0.56 (CH_2, $2H_m$). FTIR (KBr, cm^{-1}): 3361cm^{-1} (NH str.); 2966 cm^{-1} (C–CH_2–C); 1784 cm^{-1} (C=O sym. str.); 1720 cm^{-1} (C=O asym. str.); 1620 cm^{-1} (N–C=N); 1597, (C=C str. Ar.); 1504 cm^{-1} (unsym. tri-subst. Ar.); 1477 cm^{-1} (C–CH_2–C); 1441 cm^{-1} (–CH_3); 1386 cm^{-1} (C–N str. imide.); 1347–1234 cm^{-1} (Ar–O–Ar.); 1171, 1079 cm^{-1} (Si–O–C_2H_5); 1014 cm^{-1} (*para*-di-subst. Ar.); 835, 745 cm^{-1} (subst. Ar.); and 1660–1670 cm^{-1} (non PAA structure band).

$PI_{6FDA\text{-}APB(Si)}$_$HBPI_{BPADA\text{-}TAP(Si)}$_$SiO_2$ ternary composites (series SD group). The hybrid ternary composites were prepared by a typical sol-gel method (**Scheme 2**). The preparation procedure for a composite SD-3 ($PI_{6FDA\text{-}APB(Si)}$_$HBPI_{BPADA\text{-}TAP(Si)}$-20%_$SiO_2$-20%) is given here as a typical example. Stoichiometric quantities of TEOS in DMAc (10 wt%, 1.38 g), and HCl in deionised water (0.1 N, 0.048 g) were mixed and stirred at room temperature for 0.5 h to form the SiO_2 sol. Then, the SiO_2 solution was added dropwise to a stirred solution of linear $PAA_{6FDA\text{-}APB(Si)}$ (10 wt%, 2 g) and $HBPI_{BPADA\text{-}TAP(Si)}$ (0.04 g). To obtain the precursor, the solution was stirred at room temperature for 12 h. In the second stage, the precursor solution was cast onto a glass plate and heated at 80 °C for 2 h. The film was then thermally imidized by stepwise heating to 150 °C (1 h), 200 °C (1 h) and 300 °C (1 h).

The hybrid ternary composites with different compositions were prepared by a similar method, that is, by adjusting the composition of $PI_{6FDA\text{-}APB(Si)}$ and silica. The film formation property of the hybrid ternary composites depended on the contents of the $HBPI_{BPADA\text{-}TAP(Si)}$ and TEOS. By using the linear $PAA_{(Si)}$ and silane terminated hyperbranched polyimide, the hybrid ternary composites were successfully prepared. The films are labelled as SD-2 to SD-5 ($PI_{6FDA\text{-}APB(Si)}$_$HBPI_{BPADA\text{-}TAP(Si)}$-10~40%_$SiO_2$-20%). The percentage given in the generic abbreviations is the weight percentage. The hybrid ternary composites have similar spectra, and the characteristic IR absorption bands are listed below.

[SD-2 to SD-5] FT-IR (KBr, cm^{-1}): 3361cm^{-1} (–NH str.); 2910 cm^{-1} (C–CH_2–C); 1776 cm^{-1} (C=O sym. str.); 1716 cm^{-1} (C=O asym. str.); 1620 cm^{-1} (N–C=N); 1587 cm^{-1} (C=C str. arom.); 1504 cm^{-1} (asym. tri-subst. Ar.); 1477 cm^{-1} (C–CH_2–C); 1443 cm^{-1} (C=C str. Ar.); 1364 cm^{-1} (C–N–C str. imide.); 1356 cm^{-1} (–CH_3 Al.); 1296 cm^{-1} (–CF_3); 1235–1192 cm^{-1} (Ar.–O–Ar.); 1125 cm^{-1} (–CF_3); 1096–1067 cm^{-1} (Si–O–Si), 1012 cm^{-1} (*para*-di-subst. Ar.); 964 cm^{-1} (subst. Ar.); 888 cm^{-1} (Si–OH); 845–718 cm^{-1} (subst. Ar.); 680 cm^{-1} (–CF_3); and 1660–1670 cm^{-1} (non PAA structure band).

Characterisation

^{1}H NMR (600 MHz) spectra were recorded on a JEOL JNM-ECA600 NMR spectrometer. Fourier transform infrared (FT-IR) spectroscopic measurements were performed using a Magna-IR Nicolet 560 in the range 4000–450 cm^{-1} at a resolution of 0.35 cm^{-1}. Samples were measured in KBr disks. The phase transitions and thermal properties were characterised by differential scanning calorimeter (DSC), thermal gravimetric analysis (TGA) and dynamic mechanical analysis (DMA). TGA was performed with a TGA 2050 analyser (TA instrument Co.) over a heating range from 20 °C (room temperature) to 900 °C under nitrogen flow. The thermal phase transitions of the polymers were scanned by DSC 2910 (TA Instrument Co.) with a heating rate of 20 °C min^{-1} under nitrogen flow. The dielectric constants were measured using a NOVOCOOL Alpha-ANB (Novocontrol Technologies GmbH & Co. KG) dielectric analyser with silver paint electrode. The measurements were carried out at the room temperature with scan frequencies from 1 to 10^6 Hz using commercial Kapton® HN film reference (D_k = 3.81 at 100 kHz). The thickness of specimens was controlled to be in the range of 17 to 24 μm. The coefficients of thermal expansion (CTE) parallel to the film surfaces were measured using a DMA Q800 dynamic mechanical analyser (DMA, TA Instrument Co.) in extension mode over a temperature range of 25 to 320 °C with a force of 0.01 N. The size of samples was 14 mm in length, 5 mm in width and 2227 μm in thickness. UV-visible absorption spectra of films were measured on a Lambda Bio-40 spectrometer (Perkin–Elmer). A silica glass plate was used as a reference, and the thickness of specimens was less than 10 μm. Cross-sectional images of the samples were obtained by scanning electron microscopy (SEM) using a S5500 microscope (Hitachi) operating at an accelerating voltage of 5.0 kV. The cross-sectioned samples were prepared by breaking films in liquid nitrogen and sputtering with carbon nanoparticles. Dynamic mechanical analysis (DMA) measurements were performed using a TA Instruments DMA Q800-Dynamic Mechanical Analyzer in tension mode over a temperature range of 25 to 320 °C. Data acquisition and analysis of the storage modulus (E'), loss modulus (E'') and tension loss tangent ($\tan\delta = E''/E'$) were recorded automatically by the system. The sample was 14 mm in length, 5 mm in width and 19 to 28 μm in thickness. The sample was maintained under a continuous flow of nitrogen and the heating rate and frequency were fixed at 2 °C min^{-1} and 1 Hz, respectively.

Results and Discussion

Synthesis and Characterisation

To facilitate discussion, the numbered abbreviations SD-1 to SD-5 are used to denote $PI_{6FDA\text{-}APB(Si)}$_$HBPI_{BPADA\text{-}TAP(Si)}$-0%~40%_$SiO_2$-20% in the following discussion. A hyperbranched polyimide ($HBPI_{BPADA\text{-}TAP(Si)}$) having termini modified by a silane coupling agent was prepared by $A_2 + B_3$ polycondensation[30] from hydroxyl (–OH) terminated HBPI using (3-isocyanatopropyl) triethoxysilane (ICTEOS). The number average molecular weight (M_n) and polydispersity index (M_w/M_n) of $HBPI_{BPADA\text{-}TAP(Si)}$ were 2500 and 3.1, respectively. The molecular structure of $HBPI_{BPADA\text{-}TAP(Si)}$ was characterised by ^{1}H NMR and FT-IR. **Fig. 1** shows the ^{1}H NMR spectrum of $HBPI_{BPADA\text{-}TAP(Si)}$, and signal assignments are also shown. The peaks corresponding to triethoxysilane terminal groups and HBPI

main-chains are clearly identifiable. Compared with $HBPI_{BPADA-TAP(OH)}$, the signal due to –CONH– at 4.97 ppm indicates that isocyanate group of ICTEOS reacted with the terminal –OH groups of $HBPI_{BPADA-TAP(OH)}$. The two peaks at 1.15 ppm and 4.12 ppm correspond to the methyl and methylene of the ethoxy groups of ICTEOS. In addition, the methyl signals at 3.17, 1.67–1.60 ppm and 0.56 ppm correspond to the flexible $–CH_2–$ linkages in ICTEOS. It can be seen that the –OH terminal groups of $HBPI_{BPADA-TAP(OH)}$ were successfully modified with ICTEOS. This spectral evidence indicates that HBPI with silane termini has been successfully prepared. The other typical backbone resonance signals have been described in our previous work.[30]

The FT-IR spectra of $HBPI_{BPADA-TAP(Si)}$, a linear binary composite (SD-1), and hybrid ternary composites (SD-2 to SD-5) are shown in **Fig. 2**. Absorption bands of the imide groups were clearly observed for all of the composites at 1784 and 1776 cm^{-1} for the symmetric stretch and 1720 and 1716 cm^{-1} for the anti-symmetric stretching vibrations of the carbonyl group. As the amount of the $HBPI_{BPADA-TAP(Si)}$ increased, the absorption of these bands, and other characteristic bands at 1504 (asym. tri-subst. Ar.), 1356 ($–CH_3$ Al.) and 1012 cm^{-1} (*para*-di-subst. Ar.), increased significantly. No obvious absorption bands between 1660–1670 cm^{-1} due to polyamic acids (PAAs) were observed. In addition, the absorption peaks of the ethoxysilane group ($–SiOC_2H_5$) of $HBPI_{BPADA-TAP(Si)}$ were clearly visible between 1171 and 1079 cm^{-1} in the spectrum of $HBPI_{BPADA-TAP(Si)}$. The peaks assignable to $–CH_2–CH_2–$ linkage appear at 2966, 2910 and 1477 cm^{-1}. The –CONH– absorption band was found at 3361 cm^{-1}, indicating that the ICTEOS isocyanate successfully modified the –OH termini of $HBPI_{BPADA-TAP(OH)}$.

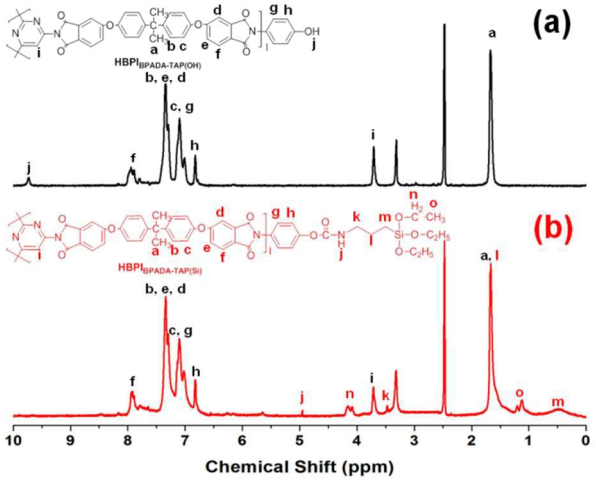

Fig. 1 ^1H NMR spectra of the (a) hydroxyl terminated hyperbranched polyimide ($HBPI_{BPADA-TAP(OH)}$)[30] and (b) the silane termini hyperbranched polyimide ($HBPI_{BPADA-TAP(Si)}$).

Due to the organosilane groups and the SiO_2 cross-linked networks derived from a cross-linking agents TEOS and terminal agents APTEOS and ICTEOS, absorption bands were observed for all the films between 1096 and 1067 cm^{-1} (Si-O-Si symmetric stretching vibrations) and 888 cm^{-1} (Si–OH), indicating that, not only were the PI precursors fully imidized, but the ternary composites (series labelled SD) were successfully prepared with inorganic silica networks.

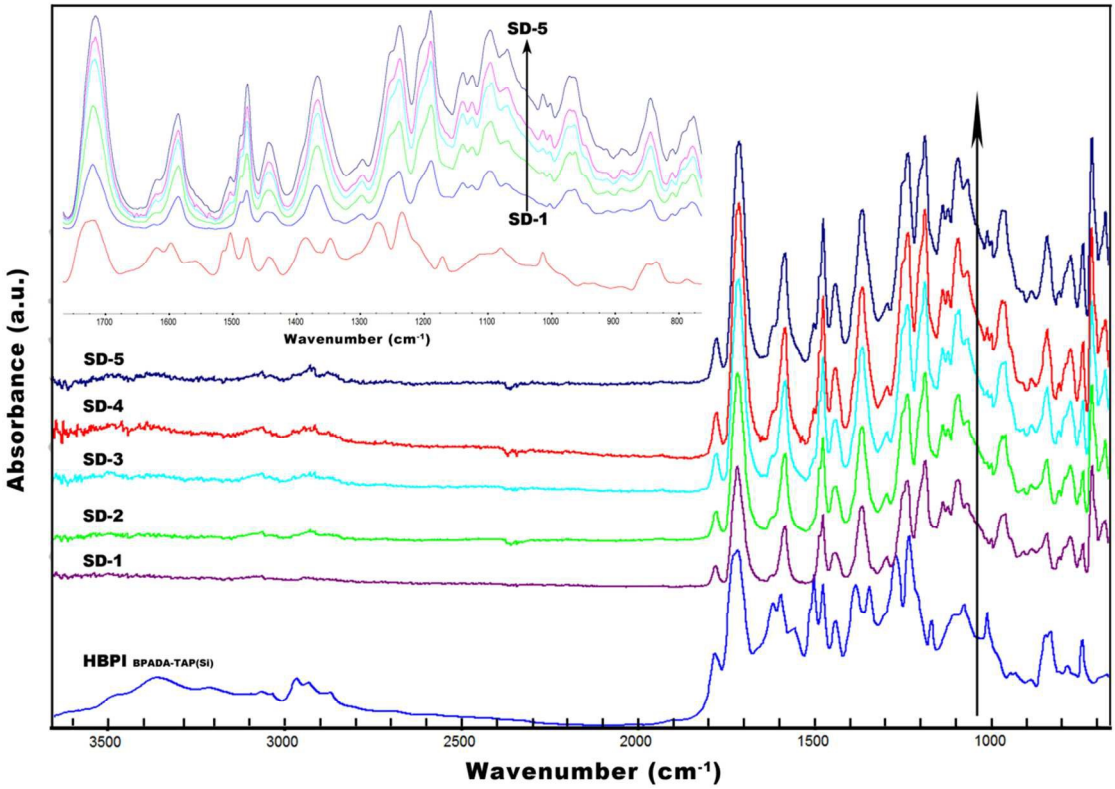

Fig. 2 FT-IR spectra of silane terminated hyperbranched polyimides, the linear binary composite (SD-1, $PI_{(Si)}$_SiO_2-20%)[32] and hybrid ternary composites (SD-2 to SD-5, $PI_{(Si)}$_$HBPI_{(Si)}$-10%~40%_SiO_2-20%).

Compared with $HBPI_{BPADA\text{-}TAP(Si)}$, the slight change in the bands due to C=O, C–N and C–O functional groups in the composite films is attributed to the increasing intermolecular interactions that occur via the strong covalent bonding of the silica terminal groups between $HBPI_{BPADA\text{-}TAP(Si)}$ and the binary composite after treatment with the TEOS linkage agent; this increased the dispersion effect in the composite matrices and led to a small displacement in their absorption peaks.

Morphology of the hybrid ternary composites

Fig. 3 shows typical cross-sectional SEM images of representative composite SA-1, SA-3, SF-4 and SD-4 films. The morphology of the films shows clear improvement in the dispersion on changing the $HBPI_{BPADA\text{-}TAP(Si)}$ and $PI_{6FDA\text{-}APB(Si)}$ composition and introducing SiO_2 cross-linkage in the matrix. The more disperse phases in the composite SD-4 are evident in **Fig. 3(d).**

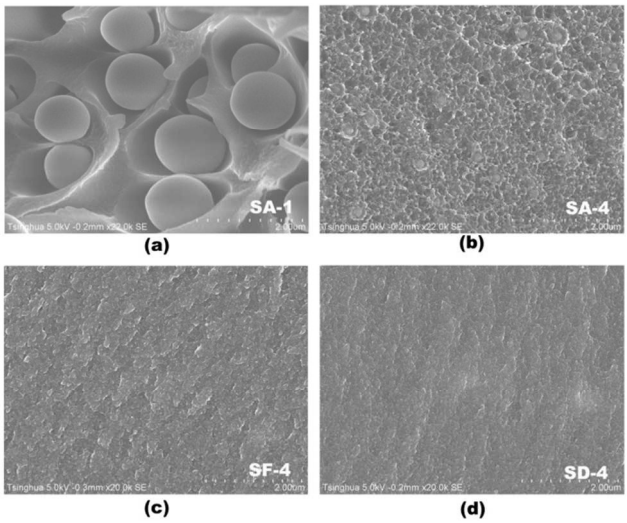

Fig. 3 Typical SEM images of PI and the composites. (a) SA-1 ($PI_{6FDA\text{-}APB}$_SiO_2-20%),[30] (b) SA-4 ($PI_{6FDA\text{-}APB}$_$HBPI_{BPADA\text{-}TAP(OH)}$-30%_$SiO_2$-20%),[30] (c) SF-4 ($PI_{6FDA\text{-}APB(Si)}$_$HBPI_{BPADA\text{-}TAP(OH)}$-30%_$SiO_2$-20%)[32] and (d) SD-4 ($PI_{6FDA\text{-}APB(Si)}$_$HBPI_{BPADA\text{-}TAP(Si)}$-30%_$SiO_2$-20%). Scale bar: 2 μm.

For the $PI_{6FDA\text{-}APB}$ and SiO_2 (SA-1 and SA-3) composites,[30] the aggregated silica particles can be clearly seen as spherical beads with a smooth polyimide surface. The beads have an average diameter of around 1500 nm in **Fig. 3(a)** and between 100 to 200 nm in **Fig 3(b)**.[30] On introduction of the triethoxysilane termini to the backbone PI, the dispersion of SiO_2 throughout the matrices dramatically improved. Compared with SA-1, SA-3[30] and SF-3,[32] SD-3 shows the smoothest cross-sectional surface and is very similar to that of PI without an inorganic component. The adhesion between the organic and inorganic components is also improved, as shown by the interface between the inorganic component and organic matrices. Moreover, the images reveal that very small nano-scaled cavities exist in the hybrid ternary composite. The enhanced interactions between the components in the ternary composites improve the dispersion of silica components and suppress the phase separation between PI and the inorganic silica networks. Because of this, light transmission through the composites was significantly improved on incorporation of $HBPI_{BPADA\text{-}TAP(Si)}$ into the $PI_{6FDA\text{-}APB(Si)}$ and SiO_2 composites. The decrease in D_k in the low frequency region (between 1 and 10^4 Hz) is primarily due to the localised orientation polarisation of the imide groups and can be attributed to the reduction in phase separation.

Dielectric properties of the hybrid ternary composites

The dielectric constants and dielectric loss of the hybrid composites (SD-1 to 5) and commercial Kapton® HN, used as a control, are shown in **Fig. 4** and listed in **Table 1**. The D_k values of the hybrid composites and related materials were measured in the frequency range of 1 to 10^6 Hz and at the fixed frequency of 100 kHz.

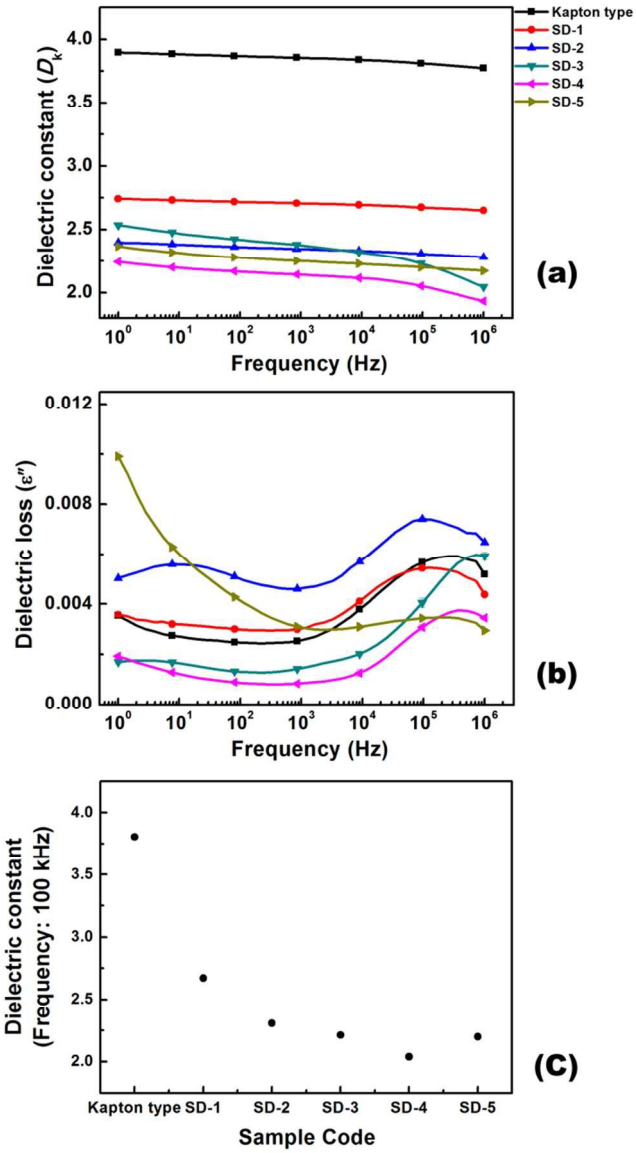

Fig. 4 Dielectric constants (D_k) of linear binary composite (SD-1, $PI_{(Si)}$_SiO_2-20%)[32] and hybrid ternary composites (SD-2 to SD-5, $PI_{(Si)}$_$HBPI_{(Si)}$-10%~40%_SiO_2-20%) (a) from 10^6 to 1 Hz, (c) at 100kHz, and (b) dielectric loss (ε″) from 10^6 to 1 Hz .

Table 1 Data for triethoxysilane termini hyperbranched polyimide with PI/SiO_2 hybrid ternary composites.

Sample	Thickness[a] μm	D_k[b]	Transmittance λ_{cutoff} nm	Transmittance 450 nm/ %	Transmittance 400 nm/ %	DSC T_g / °C	TGA $T_d^{5\%}$[c] / °C	TGA $T_d^{10\%}$[c] / °C	TGA R_{w800}[d] / %	CTE[e] ppm °C^{-1}
SD-1 $PI_{(Si)}$_SiO_2-20%	24	2.67	322	87	68	203.3	529	545	52	29.9
SD-2 $PI_{(Si)}$_$HBPI_{(Si)}$-10%_SiO_2-20%	16	2.30	323	91	79	211.2	530	545	50	28.9
SD-3 $PI_{(Si)}$_$HBPI_{(Si)}$-20%_SiO_2-20%	19	2.21	321	84	78	212.0	518	538	50	29.3
SD-4 $PI_{(Si)}$_$HBPI_{(Si)}$-30%_SiO_2-20%	33	2.04	320	95	88	212.6	516	537	51	31.4
SD-5 $PI_{(Si)}$_$HBPI_{(Si)}$-40%_SiO_2-20%	26	2.20	322	87	77	210.5	512	536	51	32.6

[a] The thickness of specimens for dielectric constant measurement.
[b] Measuring at a frequency of 100 kHz.
[c] Temperatures at which 5% and 10% weight loss occurred, recorded by TGA at a heating rate of 20 °C min^{-1} and a N_2 gas flow rate of 25 cm^3 min^{-1}.
[d] Residual weight percentages at 800 °C.
[e] The temperature range from 100 to 150 °C with a force of 0.01 N.

The dielectric constants decreased gradually with increasing frequency, and these properties are usually frequency dependent.[34] This dielectric relationship is described by the Cole-Cole equation,[35] as follows:

$$\varepsilon^* - \varepsilon_\infty = (\varepsilon_0 - \varepsilon_\infty)/[1 + (i\omega\tau_0)^{(1-\alpha)}]$$

In this equation, ε^* is the complex dielectric constant, ε_0 and ε_∞ are the dielectric constants at "static" and "infinite frequency", $\omega = 2\pi$ times the frequency, and τ_0 is a generalised relaxation time. The exponent parameter α can assume values between 0 and 1, the former corresponding to the Debye response[35] for polar dielectrics. In general, the dielectric constant of polyimide is determined by the ability of the polarisable units to orient fast enough to keep up with the applied AC voltage (100 kHz). The D_ks of all the films measured at 100 kHz are compared in **Fig. 4(c)**. The D_ks of the films prepared in this study are significantly lower than that of the linear $PI_{6FDA\text{-}APB}$ (S-1).[30]

Compared with the three series of PI composites SA,[30] SB, SC[31] and SF[32] groups reported by us, the series SD composites in the 1 Hz to 10^4 Hz range are lower D_ks shown in **Fig. 4(a)**. It may be related to a decrease in localised space-charge polarisation as well as the orientation polarisation of the imide groups being the main factor affecting the dielectric dispersion between the covalently bound organic and inorganic phases in the multi-phase matrices. It can be seen that the triethoxysilane termini of $PI_{6FDA\text{-}APB(Si)}$ and $HBPI_{BPADA\text{-}TAP(Si)}$ increases the homogeneous dispersion of silica in these systems by the formation of covalent bonds between the triethoxysilane terminal groups of $HBPI_{BPADA\text{-}TAP(Si)}$ and the linear $PI_{6FDA\text{-}APB(Si)}$ backbone by the TEOS cross-linking agent. In comparison to series SA[30] and SF[32], the series SD composites showed good adhesion between the silica and the PI matrix because of the terminal linkages on $PI_{6FDA\text{-}APB(Si)}$ and the reaction of $HBPI_{BPADA\text{-}TAP(Si)}$ with TEOS. The D_k values of the hybrid ternary composites (SD-2 to SD-5) are smaller than that of the binary composite (SD-1). Under the optimised conditions, SD-4 had the smallest D_k of the composites of 2.04, significantly lower than either SA-4 (a typical specimen in SA series, D_k = 2.24)[30] and SF-4 (a typical specimen in SF series, D_k = 2.19).[32] This can be attributed to the terminal linkages of $HBPI_{BPADA\text{-}TAP(Si)}$ that promote homogeneous dispersion, increased free volume[44] and good miscibility through their covalent bonds. In our hybrid ternary composite series, the organosilane termini of $HBPI_{BPADA\text{-}TAP(Si)}$ promotes phase dispersion, and plays an important role in reducing the dielectric constant in the hybrid ternary composites.

Optical properties of the hybrid ternary composites

The optical transparency of series SD group was measured with a UV-vis spectrometer. **Fig. 5** shows the UV-vis transmission spectra. The cut-off wavelengths (absorption edge, λ_{cutoff}) and the transmissions at 450 nm and 400 nm in these spectra are listed in **Table 1**.

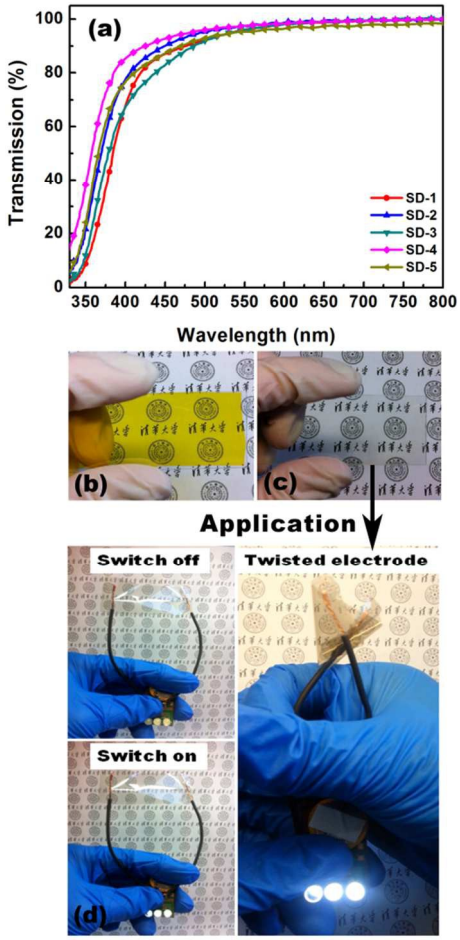

Fig. 5 Optical transmission (a) of the linear binary composite (SD-1, $PI_{(Si)}$_SiO_2-20%)[32] and hybrid ternary composites (SD-2 to SD-5, $PI_{(Si)}$_$HBPI_{(Si)}$-10%~40%_SiO_2-20%) measured from 800 to 320 nm. Photographs of (b) Kapton® HN, (c) SD-4 hybrid ternary composite film and (d) the applied electrode model.[43]

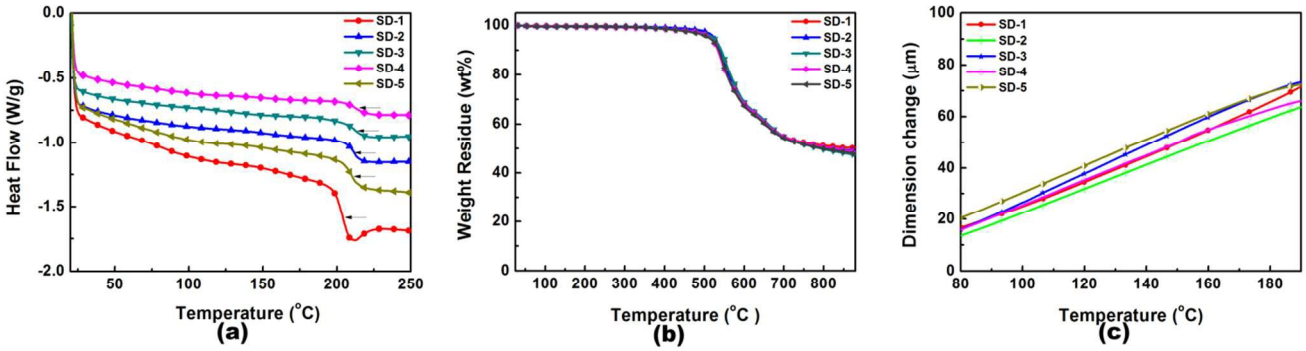

Fig. 6 DSC (a), TGA (b) and CTE(c) spectra of the linear binary composite (SD-1, $PI_{(Si)}$_SiO_2-20%)[32] and the hybrid ternary composites (SD-2 to SD-5, $PI_{(Si)}$_$HBPI_{(Si)}$-10%~40%_SiO_2-20%)

The optical transparency of the series SD composites is clearly improved by incorporating $HBPI_{BPADA\text{-}TAP(Si)}$ into the $PI_{6FDA\text{-}APB(Si)}$_SiO_2 system. The optical transmissions of the SD group increased from 84% to 95% at 450 nm and from 68% to 88% at 400 nm, respectively. By incorporating $HBPI_{BPADA\text{-}TAP(Si)}$, SD-4 showed the highest transmission, i.e. 95% at 450 nm and 88% at 400 nm, higher than SA-4 ($PI_{6FDA\text{-}APB}$_$HBPI_{BPADA\text{-}TAP(OH)}$-10%_$SiO_2$-20%)[30] and SF-4 ($PI_{6FDA\text{-}APB(Si)}$_$HBPI_{BPADA\text{-}TAP(OH)}$-10%_$SiO_2$-20%).[32] The higher optical transparency is observed in the specimens with highly dispersed phases, as confirmed by the SEM cross-sectional images. In addition, the composites maintain the fundamental characteristics of the monomers, i.e., the high fluorine content of 6FDA,[36,37] the flexible and bent structure of APB[38,39] and the bulky side groups of BPADA.[40–42] These are all important for the formation of a colourless film. In addition, the high optical transmission can be attributed to the synergistic effect between the $HBPI_{BPADA\text{-}TAP(Si)}$ and $PI_{6FDA\text{-}APB(Si)}$ components that reduces phase separation between the PI matrices and silica particles, improving dispersibility and reducing the size of the silica particles. Therefore, light scattering in the visible region from aggregation of the inorganic silica phase is effectively suppressed.

Thermal properties of the hybrid ternary composite films

The thermal phase transition behaviour of the hybrid composites and related materials was investigated by DSC. The results are shown in **Fig. 6(a)** and summarised in **Table 1**. All the hybrid ternary composites and related materials have defined glass transition temperatures, indicating that the PI components exist in an amorphous phase.

The SD group composites have glass transition temperatures (T_g) ranging from 203.3 to 212.6 °C. The T_g of the binary composite with 20 wt% SiO_2 (SD-1) is 203.3 °C. Even better, enhanced T_gs were observed for the hybrid ternary composites prepared with $HBPI_{BPADA\text{-}TAP(Si)}$, attributed to the covalent cross-linked networks. The T_g of SD-4 is 212.6 °C, the highest of the ternary composite series. On the other hand, the T_g of SD-5 is 210.5 °C, the lowest in the ternary composite series, and this is due to its hyperbranched structure and the low molecular weight of $HBPI_{BPADA\text{-}TAP(Si)}$. The slightly lower T_g of SD-5 can be attributed to its large free volume and the low T_g of the hyperbranched polymer. On the other hand, as long as the concentration of $HBPI_{BPADA\text{-}TAP(Si)}$ is below the critical value, segregation from the matrices does not occur nor is the T_g affected significantly. However, the cause of the lower T_g value for SD-5 is not obvious.

The thermal decomposition temperatures of the hybrid ternary composites and related materials measured by TGA are shown in **Fig. 6(b)** and summarised in **Table 1**. For the SF series, the residual weights of the composites were nearly 100% at temperatures less than 500 °C, significantly higher than those of the SA, SB, SC and SD series.[23,24] The 5% and 10% weight loss temperatures ($T_d^{5\%}$ and $T_d^{10\%}$) of SD-1 are 529 °C and 545 °C, respectively. The ternary hybrid composites (SD-2 to SD-5) have $T_d^{5\%}$ values ranging from 530 to 512 °C and $T_d^{10\%}$ values ranging from 545 to 536 °C. These are significantly higher than those of the SA series are ($T_d^{5\%}$: 487 to 481 °C).[30] This difference between SA and SD series can be attributed to the terminal cross-linked silica networks between $HBPI_{BPADA\text{-}TAP(Si)}$ and $PI_{6FDA\text{-}APB(Si)}$. The T_d values decreased with increasing $HBPI_{BPADA\text{-}TAP(Si)}$ content in the systems, which might be caused by the elimination of water molecules from Si–OH group of $HBPI_{BPADA\text{-}TAP(Si)}$ at high temperatures.

The coefficient of thermal expansion (CTE) was characterised by DMA in the direction of film surface of the ternary hybrid composites and related materials. The CTE curves are shown in **Fig. 6(c)** and the CTE values in the temperature range from 100 to 150 °C are listed in **Table 1**.

The CTE values of the SD series change from 32.6 to 28.9 ppm $°C^{-1}$. By comparing the CTE values at temperatures below the T_g, the hybrid composites exhibit significantly smaller CTEs than that of the pristine PI (S-1, 37.1 ppm $°C^{-1}$).[30] The smallest CTE value was obtained for SD-1 (28.9 ppm $°C^{-1}$). This can also be attributed to the cross-linkages formed between the silica terminal groups of $HBPI_{BPADA\text{-}TAP(Si)}$ and $PI_{6FDA\text{-}APB(Si)}$ in composites with a well-designed content ratio. However, compared to the CTE of 17.8 ppm $°C^{-1}$ for SA-1 ($PI_{6FDA\text{-}APB}$_SiO_2-20%),[30] the CTE values are larger. Furthermore, they also increase with the further increase in $HBPI_{BPADA\text{-}TAP(Si)}$ content. This may be a negative effect of the triethoxysilane termini of $PI_{6FDA\text{-}APB(Si)}$ and $HBPI_{BPADA\text{-}TAP(Si)}$ compared with $PI_{6FDA\text{-}APB}$ and $HBPI_{BPADA\text{-}TAP(OH)}$, which could increase the inter-chain distances and form nano-scale cavities.[29,44,45] In spite of the incorporation of $HBPI_{BPADA\text{-}TAP(Si)}$, the effect of the covalent linkages in reducing CTE is offset by the $PI_{6FDA\text{-}APB(Si)}$ and $HBPI_{BPADA\text{-}TAP(Si)}$ components. This tendency can be seen by comparing the CTEs among the series SA and SF groups. Even in

this case, the CTEs of the ternary hybrid composites are still much smaller than that of typical linear PI (S-1). [30] The results shown above indicate that these hybrid ternary composites show significant improvements in their dielectric properties and have high transparency, properties that are attained by the introduction of $HBPI_{BPADA\text{-}TAP(OH)}$ in the $PI_{6FDA\text{-}APB(Si)}$-20% and SiO_2 composites.

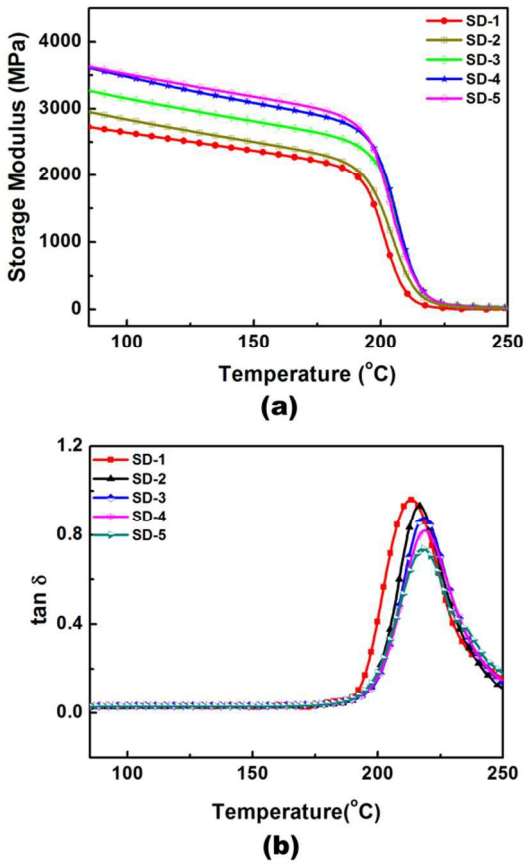

Fig. 7 (a) Storage moduli (MPa) and (b) tan δ spectra of the linear binary composite (SD-1, $PI_{(Si)}\_SiO_2$-20%) and the hybrid ternary composites (SD-2 to SD-5, $PI_{(Si)}\_HBPI_{(Si)}$-10%~40%_SiO_2-20%)

Table 2 Storage moduli (MPa), tan δ and T_gs values of the linear binary composite (SD-1, $PI_{(Si)}\_SiO_2$-20%) and the hybrid ternary composites (SD-2 to SD-5, $PI_{(Si)}\_HBPI_{(Si)}$-10%~40%_SiO_2-20%)

Sample	Storage modulus at 100 °C	Storage modulus at 180 °C	tan δ	T_g
	MPa	MPa		°C
SD-1	2643.8	2174.4	0.96	213.2
SD-2	2840.1	2276.8	0.93	216.7
SD-3	3153.2	2599.0	0.87	218.0
SD-4	3477.9	2859.1	0.82	218.8
SD-5	3517.5	2952.0	0.73	217.2

Mechanical properties of the hybrid ternary composite films

The temperature variation of the storage modulus (E') and phase angle (tan δ, the ratio of loss modulus (E'') to storage modulus (E')) for SD-1 and SD-2 to SD-5, which were measured by DMA analysis, are listed in **Table 2** and shown in **Fig. 7**. In comparison with a binary composite (SD-1), the ternary composites (SD-2 to SD-5) had enhanced storage moduli (E'), higher T_g temperatures and reduced tan δ values and these changes correlated with increasing $HBPI_{BPADA\text{-}TAP(Si)}$ content. The increase in E' is indicative of the enhanced strong interfacial interactions due to covalent bonds between $HBPI_{BPADA\text{-}TAP(Si)}$ and $PI_{6FDA\text{-}APB(Si)}\_SiO_2$ in the binary composite. These enhanced interactions are caused by the cross-linking reactions between the triethoxysilane terminal groups and TEOS in the two-step network forming process as the hydrolysis and polycondensation reaction occur at elevated temperature. SD-5 has the largest storage modulus of 2952.0 MPa at 180 °C. The values from 0.96 to 0.73 of tan δ for the composite films decrease with increasing $HBPI_{BPADA\text{-}TAP(Si)}$ content. We also observed enhanced elastic behaviour of the composite films (SD-2 to SD-5) in comparison with the $PI_{6FDA\text{-}APB(Si)}\_SiO_2$ binary composite matrix. This is attributable to the strong interfacial interactions of the covalent linkages between the organic and inorganic phases.

Conclusions

We successfully synthesised an organosilane terminated hyperbranched polyimide ($HBPI_{BPADA\text{-}TAP(Si)}$) by using a (3-isocyanatopropyl) triethoxysilane (ICTEOS) agent that was introduced by modification of the –OH group at the peripheral positions of $HBPI_{BPADA\text{-}TAP(OH)}$.

Based on the linear $PI_{6FDA\text{-}APB(Si)}$ and hyperbranched $HBPI_{BPADA\text{-}TAP(Si)}$ that have triethoxysilane termini, hybrid ternary composites (SD series) were fabricated by a sol-gel cross-linking reaction with TEOS. The hybrid ternary composites had desirable dielectric properties. At an appropriate content of $HBPI_{BPADA\text{-}TAP(Si)}$, the dielectric constant (D_k) of SD-4 ($PI_{6FDA\text{-}APB(Si)}\_HBPI_{BPADA\text{-}TAP(Si)}$-30%_$SiO_2$-20%) had the lowest D_k of the series, 2.04. The optical transparency of the ternary hybrid composite films was also improved due to the synergistic interaction between $HBPI_{BPADA\text{-}TAP(Si)}$ and $PI_{6FDA\text{-}APB(Si)}$ that reduced phase separation. The best result was obtained for SD-4 in the ternary hybrid composites, for which the corresponding transmittance increased from 87% for SD-1 ($PI_{6FDA\text{-}APB(Si)}\_SiO_2$-20%) to 95% at 450 nm. The incorporation of the strongly covalent terminal networks of $HBPI_{BPADA\text{-}TAP(Si)}$ and $PI_{6FDA\text{-}APB(Si)}\_SiO_2$-20% improves the thermal stability of the binary composites. The T_g of SD-4 was 212.6 °C, which is the highest of the ternary composite series. The CTE value of SD-2 ($PI_{6FDA\text{-}APB(Si)}\_HBPI_{BPADA\text{-}TAP(Si)}$-10%_$SiO_2$-20%, 28.9 ppm $°C^{-1}$) was the smallest in the hybrid ternary composites. The triethoxysilane termini of $PI_{6FDA\text{-}APB(Si)}$ and $HBPI_{BPADA\text{-}TAP(Si)}$ did not further reduce the CTE values. SD-5 has the largest storage modulus (E'), 2952.0 MPa at 180 °C. The values of tan δ for the composite films decrease with increasing $HBPI_{BPADA\text{-}TAP(Si)}$ content. In general, the hybrid ternary composites with strongly cross-linked SiO_2 covalent bonding networks developed in this study show improved dielectric, optical, thermal and mechanical propertiese. These results are promising, allowing the development of new materials with high performance that meet the technical requirements for interlayer dielectrics in advanced electronic devices.

Acknowledgement

The financial support from National Basic Research Program of

China (973 Program) under Project 2011CB606102 is gratefully acknowledged.

Reference

1. Y. Jin, L. Li, Y. Cheng, L. Kong, Q. Pei and F. Xiao, *Adv. Funct. Mater.*, 2015, **25**, 1581.
2. Y. Kim, S. Cook, S. M. Tuladhar, S. A. Choulis, J. Nelson, J. R. Durrant, D. D. C. Bradley, M. Giles, I. Mcculloch, C. S. Ha and M. H. Ree, *Nat. Mater.*, 2006, **5**, 197.
3. S. Nam, M. Shin, H. Kim, C. S. Ha, M. H. Ree and Y. Kim, *Adv. Funct. Mater.*, 2011, **21**, 4527.
4. M. C. Choi, Y. K. Kim and C. S. Ha, *Prog. Polym. Sci.*, 2008, **33**, 581.
5. D. Sun, M. Y. Timmermans, Y. Tian, A. G. Nasibulin, E. I. Kauppinen, S. Kishimoto, T. Mizutani and Y. Ohno, *Nat. Nanotech.*, 2011, **6**, 156.
6. H. Lim, W. Cho, C. S. Ha, S. Ando, Y. K. Kim, C. H. Park and K. Lee, *Adv. Mater.*, 2002, **18**, 1275.
7. L. Li, Z. Yu, C. Chang, W. Hu, X. Niu, Q. Chen and Q. Pei, *Phys. Chem. Chem. Phys.*, 2012, **14**, 14249.
8. Z. Zhang, K. Guo, Y. Li, X. Li, G. Guan, H. Li, Y. Luo, F. Zhao, Q. Zhang, B. Wei, Q. Pei and H. Peng, *Nat. Photonics*, 2015, **9**, 233.
9. Y. Yuan, F. S. Riehle, R. Nitschke and M. Krügera, *Mater. Sci. & Eng. B*, 2012, **177**, 245.
10. W. Volksen, R. D. Miller and G. Dubois, *Chem. Rev.*, 2010, **110**, 56.
11. Y. H. Zhang, S. G. Lu, Y. Q. Li, Z. M. Dang, J. H. Xin, S. Y. Fu, G. T. Li, R. R. Guo and L. F. Li, *Adv. Mater.*, 2005, **17**, 1056.
12. H. Chen, L. Xie, H. Lu and Y. Yang, *J. Mater. Chem.*, 2007, **17**, 1258.
13. D. J. Liaw, K. L. Wang, Y. C. Huang, K. R. Lee, J. Y. Lai and C. S. Ha, *Prog. Polym. Sci.*, 2012, **37**, 907.
14. P. Tapaswi, M. C. Choi, K. M. Jeong, S. Ando, C. S. Ha, *Macromolecules*, 2015, **48**, 3462.
15. Y. Terui and S. Ando, *J. Appl. Phys.*, 2014, **116**, 53524-1.
16. J. H. Wu and G. S. Liou, Adv. Funct. Mater., 2014, **24**, 6422.
17. H. J. Yen, J. H. Wu, Y. H. Huang, W. C. Wang, K. R. Lee and G. S. Liou, *Polym. Chem.*, 2014, **5**, 4219.
18. Y. T. Chern and J. Y. Tsai, *Macromolecules*, 2008, **41**, 9556.
19. J. C. Huang, P. C. Lim, L. Shen, P. K. Pallathadka, K. Y. Zheng and C. B. He, *Acta Mater.*, 2005, **53**, 2395.
20. H. J. Yen, J. H. Wu, W. C. Wang and G. S. Liu, *Adv. Opt. Mater.*, 2013, **1**, 688.
21. H. Lim, C. Bae, J. Park, W.J. Cho and C.S. Ha, *Synth. Metal.*, 2003, **137**, 1017.
22. H. Deligöz, S. Özgümüş, T. Yalçınyuva, S. Yildirim, D. Deger and K. Ulutas, *Polymer*, 2005, **46**, 3720.
23. G. S. Liou, Y. L. Yang and Y. O. Su, *J. Polm. Sci.: Part A*, 2006, **44**, 2587.
24. G. F. Zhao, T. Ishizaka, H. Kasai, M. Hasegawa, T. Furukawa, H. Nakanishi and H. Oikawa, *Chem. Mater.*, 2009, **21**, 419.
25. J. H. Wu and G. S. Liou, ACS Appl. Mater. Inter., 2015, **7**, 15988.
26. V. E. Yudin, J. U. Otaigbe, S. Gladchenko, B. G. Olson, S. Nazarenko, E. N. Korytkova and V. V. Gusarow, *Polymer*, 2007, **48**, 1306.
27. E. Hamciuc, C. Hamciuc and M. Olariu, *Polym. Engin. & Sci.*, 2009, **50**, 520.
28. H. W. Wang, R. X. Dong, H. C. Chu, K. C. Chang and W. C. Lee, *Mater. Chem. & Phys.*, 2005, **94**, 42.
29. Y. J. Lee, J. M. Huang, S. W. Kuo, and F. C. Chang, *Polymer*, 2005, **46**, 10056.
30. S.K. Kim, X.Y. Wang, S. Ando and X.G. Wang, *RSC Adv.*, 2014, **4**, 27267.
31. S.K. Kim, X.Y. Wang, S. Ando and X.G. Wang, *RSC Adv.*, 2014, **4**, 42737.
32. S.K. Kim, X.Y. Wang, S. Ando and X.G. Wang, *RSC Adv.*, 2015, **5**, 40046.
33. S.K. Kim, X.Y. Wang, S. Ando and X.G. Wang, *Eur. Polym. J.*, 2015, **64**, 206.
34. J. O. Simpson and A. K. St.Clair, *Thin Solid Films*, 1997, **308-309**, 480.
35. K. S. Cole and R. H. Cole, *J. Chem. Phys.*, 1941, **9**, 341.
36. G. Hougham, G. Tesoro and J. Shaw, *Macromolecules*, 1995, **27**, 3642.
37. A. E. Feiring, B. C. Auman and E. R. Wonchoba, *Macromolecules*, 1993, **26**, 2779.
38. G. C. Eastmond and J. Paprotny, *Macromolecules*, 1995,**28**, 2140.
39. Y. Imai, *High Perform. Polym.*, 1995, **7**, 337.
40. Y. T. Chern and H. C. Shiue, *Macromolecules*, 1997, **30**, 4646.
41. L. J. Mathias, A. V. G. Muir and V. R. Reichert, *Macromolecules*, 1991,**24**, 5232.
42. X. T. Han, Y. Tian, L. H. Wang and C. F. Xiao, *J. Appl. Polym. Sci.*, 2008, **107**, 618.
43. S. K. Kim, T. Liu and X. G.Wang, *ACS Appl. Mater. & Interfaces*, 2015, **7**, 20865..
44. T. Suzuki and Y. Yamada, *High Perform. Polym.*, 2007, **19**, 553.
45. T. Seçkin, S. Köytepe and H. I. Adıgüzel, *Mater. Chem. & Phys.*, 2008, **112**, 1040.

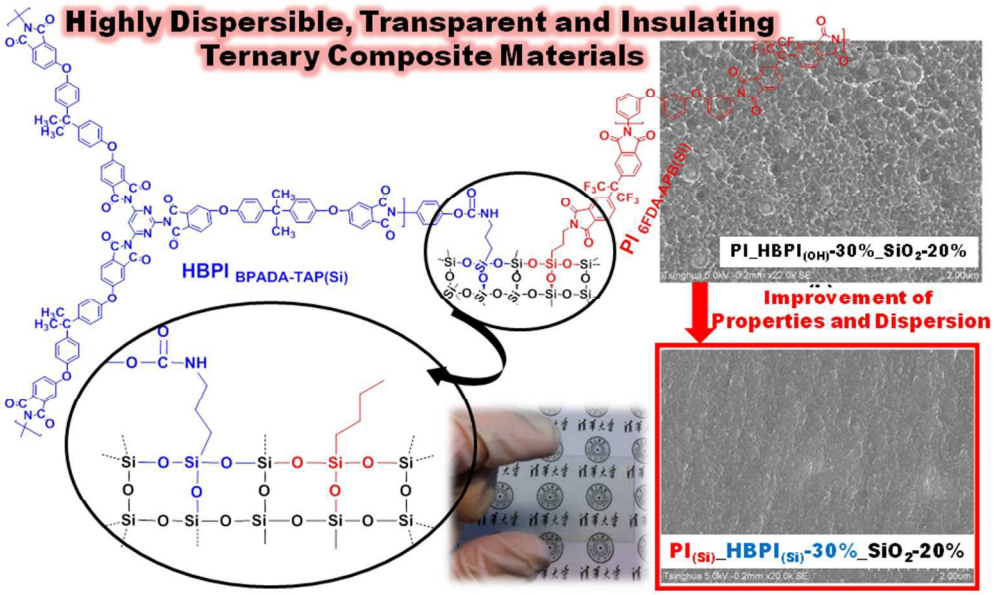

253x153mm (96 x 96 DPI)